Energy & Buildings 197 (2019) 120–130

Contents lists available at ScienceDirect

Energy & Buildings

journal homepage: www.elsevier.com/locate/enbuild

Experimental and numerical investigation of a high-efficiency dew-point evaporative cooler

Yuting Liu[a], Yousef Golizadeh Akhlaghi[b], Xudong Zhao[b], Junming Li[a,*]

[a] Key Laboratory for Thermal Science and Power Engineering of Ministry of Education, Department of Energy and Power Engineering, Tsinghua University, Beijing 100084, China
[b] School of Engineering, University of Hull, HU6 7RX, UK

ARTICLE INFO

Article history:
Received 8 February 2019
Revised 9 May 2019
Accepted 14 May 2019
Available online 15 May 2019

Keywords:
Dew-point
Evaporative cooler
Experimental study
Numerical study
Optimization

ABSTRACT

This paper investigated the cooling performance of a high-efficiency dew-point evaporative cooler with optimised air and water flow arrangement using the combined experimental and numerical simulation method. The experimental results showed that the wet-bulb efficiency of the dew-point evaporative cooler was increased by 29.3% and COP was increased by 34.6%, compared to the existing commercial dew point air cooler of the same capacity. An improved two-dimensional, multi-factor engaged numerical model which can scale up and optimize the size and capacity of the cooler was developed. The numerical predictions agreed well with the experimental results, indicating that the cooling rate of the dew-point evaporative cooler is influenced by the dew-point evaporative cooler structure. The cooling efficiency of the dew-point evaporative cooler with corrugated plates is more than 10% higher than with flat plates and the cooling efficiency of the dew-point evaporative cooler with the actual flow arrangement is only 62%–67% that of a dew-point evaporative cooler with an ideal counter-flow arrangement. The cooling efficiency can be improved by increasing the channel length and the air entrance length, and decreasing the channel width and channel gap within a reasonable range.

1. Introduction

Evaporative cooling is an energy-saving and environmentally-friendly cooling technology where the heat is absorbed and the air is cooled through water evaporation. Evaporative cooling methods can be divided into direct evaporative cooling (DEC) and indirect evaporative cooling (IEC) according to whether or not the product air is in contact with water. The IEC systems have an additional sensible heat exchange channel which is called the dry channel compared to DEC systems which have only a wet channel where the air contacts the water directly. Therefore, IEC systems have more applications than DEC systems because the product air (also called the supply air) is cooled without being added with moistures [1]. The air in the dry channel is called the primary air while the air in the wet channel is called the secondary air or working air. The product air can be cooled to the wet-bulb temperature of the incoming air for an ideal system, but the actual wet-bulb efficiencies of DEC systems are 40–80% and the cooling capacities are largely dependent on the incoming air properties [2]. The cooling efficiency can be improved by using dew-point evaporative cooling (also called M-cycle IEC) that improves the IEC design [3–5]. In this design, the secondary air is first cooled in the dry channel before entering the wet channel so that the product air temperature can be lowered to the dew point of the incoming air for an ideal design. The wet-bulb efficiencies of M-cycle IEC systems are 10–30% higher than those of IEC systems [4].

The cooling rates and energy efficiencies of M-cycle IEC systems are influenced by the M-cycle IEC system design, so many researchers have proposed various structures for M-cycle IEC systems. Hsu et al. [6] compared the efficiencies of three different heat exchanger structures and found that the product air can easily be cooled to below the wet-bulb temperature of the incoming air and can be cooled close to the dew-point temperature of the incoming air by optimizing the system design. Lee et al. [7] optimized the dew-point evaporative cooler design and compared the efficiencies of three types of dew-point evaporative coolers with cross-flow flat plates, cross-flow corrugated plates and counter-current flow finned channels. Zhan et al. [8] studied the efficiencies of cross-flow and counter-flow dew-point evaporative coolers numerically and experimentally. Their results showed that the cooling capacity of a counter-flow dew-point evaporative cooler is about 20% higher than of a cross-flow type for the same operating conditions and same cooler volume and that the dew-point and wet-bulb efficiencies of counter-flow coolers are 15%–23% higher than those of cross-flow coolers. However, the cross-flow

* Corresponding author.
E-mail addresses: lijm@tsinghua.edu.cn, lijm@mail.tsinghua.edu.cn (J. Li).

https://doi.org/10.1016/j.enbuild.2019.05.038
0378-7788/

Nomenclature

A	Wetted surface area (m^2)
COP	Coefficient of performance
c_p	Specific heat at constant pressure (kJ/(kg•K))
d	Humidity (kg/kg)
D_{ab}	Mass diffusivity, (m^2/s)
D_e	Equivalent diameter (m)
h	Convective heat transfer coefficient (W/(m^2•K))
h_{la}	Latent heat of water evaporation (J/kg)
h_t	Overall heat transfer coefficient between the primary air and water film (W/(m^2•K))
$h_v(t_f)$	Specific enthalpy of the water film at temperature t_f (J/kg)
$h_v(t_w)$	Specific enthalpy of working air at temperature t_w (J/kg)
h_m	Mass transfer coefficient (kg/(m^2•K))
k	Thermal conductivity (W/(m•K))
l_c	Channel length (m)
l_d	Dry channel gap (m)
l_e	Characteristic length (m)
l_w	Wet channel gap (m)
m_f	Water mass flow rate (kg/s)
m_a	Air mass flow rate (kg/s)
$\dot{m}_{w,c}$	Water consumption (kg/s)
n	Number of channels
Nu	Nusselt number
p	Pressure (kPa)
Pr	Prandtl number
$Q_{coolling}$	Cooling capacity (W)
Pw	Fan and water pump power in the dew-point evaporative cooler
r	Working-to-primary air ratio
Re	Reynolds number
t	Temperature (°C)
T	Temperature (K)
u	Velocity (m/s)
V	volume of wetted media (m^3)
$V_{h,e}$	Evaporator volumetric air flowrate (m^3)
W	Channel width (m)
We_l	Weber number for the liquid phase
x	Vapour fraction

Greek symbols

ε	Cooling efficiency
Γ	Water mass flow velocity (kg/ (m•s))
δ	Thickness (m)
μ	Viscosity (kg/(m•s))
ν	Kinematic viscosity (m2/s)
ρ	Density (kg/m^3)
$\rho_{a,w}$	Dry air density of working air in the wet channel (kg/m^3)
ϕ	Heat source for the energy equation (W/m^3)
ϕ_m	Mass source for the mass equation (kg/m^3)

Subscripts

a	Air
d	Dry channel air (primary air)
db	Dry-bulb
dp	Dew point
f	Water film
g	Gravity
in	Inlet
l	Liquid phase
Le	Lewis number, k / ($\rho c_p D$)
out	Outlet
pl	Plate
po	Porous layer
s	Saturation near the water surface
t	Total
w	Wet channel air
wb	Wet-bulb

dew-point evaporative cooler has a higher energy efficiency COP, which is 10% higher than that of a counter-flow type. Riangvilaikul et al. [9, 10] measured the performance of a counter-flow flat dew-point evaporative cooler for various incoming air temperatures and humidities. Their results showed that the wet-bulb efficiency was between 92% and 114% and the dew-point efficiency was between 58% and 84%. Kabeel and Abdelgaied [11] experimentally studied a counter-flow dew-point evaporative cooler with a baffle in the dry channel. Lee and Lee [12] experimentally studied the cooling in a dew-point evaporative cooler with ribs in the wet and dry channels. Xu et al. [13] experimentally studied the cooling efficiency and energy efficiency of a high-performance counter-flow dew-point evaporative cooler for typical meteorological conditions of various regions. Their results showed that the wet-bulb efficiency range was 100–109.8% while the dew-point efficiencies were 67–76.3%. Anisimov and his team have optimized the designs of various dew-point evaporative coolers, including cross-flow and counter-flow patterns, designs with various channel structures, and various secondary air distribution methods [14–21]. As for the existing commercial dew-point evaporative cooler, the Coolerado Cooler™ with a cross-flow configuration, manufactured by Idalex, has been marketed to the residential and small commercial sector [22,23]. The dew-point evaporative cooler products of the Coolerado have developed to M50, C60 from the first product of M30. According to the lab evaluation of the Coolerado, the wet-bulb efficiency of the cooler ranged from 81% to 91% (averaging 86%) with the COP ranging from 9.3 to 40.5. [22,23].Though many researchers have proposed various dew-point evaporative cooler systems, the efficiencies of these dew-point evaporative coolers are still not very high which leads to large, costly designs. Thus, the dew-point evaporative cooler designs need to be further optimized.

The fabrication of a dew-point evaporative cooler is a complicated, time-consuming task, so the influences of various structures should be studied numerically rather than experimentally after the numerical models have been bell verified against experimental data. Zhao et al. [24] numerically studied the influences of channel length, width and gap on the efficiency of a counter-flow dew-point evaporative cooler using an algebraic model. Cui et al. [25,26] improved that model by considering more factors and numerically studied the cooling rates of dew-point evaporative coolers with various structures using the Ansys Fluent solver. Lin et al. [27,28] proposed an unsteady one-dimensional numerical model to study a dew-point evaporative cooler that neglected the influence of the water. Many models have been proposed by various researchers [29–35], but those models neglected many factors such as the influence of the water, the uneven flow of the air and conduction along the air flow direction. So, the structure optimization could not be studied using these models. More accurate models are needed to effectively optimize dew-point evaporative coolers.

Overall, the existing commercial dew-point evaporative coolers are relatively less energy efficient, leading to a large-sized and high cost operation because of unreasonable air and water flow arrangement. On the other side, the dew-point evaporative coolers previously studied in lab have smaller cooling capacities and

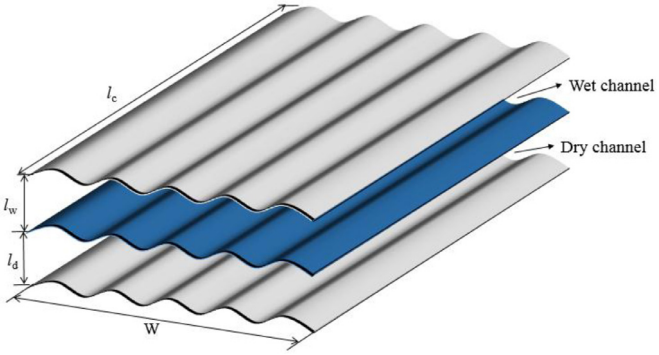

Fig. 1. Corrugated heat plates model (cooling unit model).

thus are inappropriate to site application. In this paper, a high-efficiency dew-point evaporative cooler was designed and established with improved air and water flow arrangement where the primary air and water and secondary air are closer to counter flow compared to existing commercial dew-point evaporative coolers and aluminum corrugated heat exchange plates and high wettability porous fiber placed on wet channel wall are used to increase the heat and mass transfer area and the channel supports in channels which can lead to air flow resistance are removed for the proposed dew-point evaporative cooer. To further enable the large scale and wide range applications of the dew-point evaporative coolers in real projects, this research also developed an improved two-dimensional, multi-factor engaged numerical model which can scale up and optimize the size and capacity of the unit to meet various requirements of real projects. The model itself has a few distinct advantages compared to existing models, namely, the air momentum equation and water flow equation are included and solved simultaneously with the air energy and mass transfer equations, and specific heat and mass transfer correlations for wet air is adopted in the energy and mass transfer equations. Further, the model was experimentally validated and refined by using the data obtained from coolers' testing by the authors, and thus, can guarantee its reliability and accuracy in the prediction and optimization.

2. Dew-point evaporative cooler experimental set-up

The cooling performance of a dew-point evaporative cooler design can be improved by (1) enlarging the heat exchanger heat and mass transfer area, (2) reducing the air flow resistance in the channel, and (3) making the air flow as close to ideal counter-flow as possible. These guidelines were used to design a counter-flow dew-point evaporative cooler with corrugated plates.

2.1. Dew-point evaporative cooler

A high wettability porous fiber was placed in the wet channel wall to enlarge the wetted area with the corrugated plates used to increase the volumetric heat and mass transfer area. The heat exchanger was made of aluminum to reduce the weight and to eliminate the channel supports which increase the flow resistance. The corrugated plate geometry is shown in Fig. 1 and the entire dew-point evaporative cooler design with the corrugated plates shown in Fig. 2. The bottom part of the plate was flat for the air inlet. The primary air entered the dry channel from the bottom and flowed along the dry channels while being cooled by the water film flowing down along the plate in the adjacent wet channels. Then, part of primary air was delivered to the conditioned space from the upper end of the dry channel as the product air while the other part flowed into the adjacent wet channel as the working air through the interconnecting holes in the upper part of the plate. The water flowed downwards from the water distributor at the top of the wet channel along the wet surface covered with the porous fiber where the water contacts and transfers heat and mass with working air and absorbs the sensible heat from the primary in dry channel through the wall. The enthalpy and humidity of the working air both increase until the air is discharged to the outdoors at the bottom of the wet channel as exhaust air. The detailed parameters of the dew-point evaporative cooler are listed in Table 1.

Table 1
Detailed parameters of the dew-point evaporative cooler.

Parameter	Value
Channel length (m)	1.05
Channel width W (m)	0.716
Channel gap (mm)	4.3
Air entrance length (mm)	175
Number of dry channels	117
Number of wet channels	117

2.2. Experimental set-up

A schematic of the testing system is shown in Fig. 3 and the fabricated dew-point evaporative cooler is shown in Fig. 4. The system was tested in a constant temperature and humidity lab where the temperature and humidity could be adjusted as required. The product air and the working air flow rates were controlled by adjusting the supply and exhaust air fan speeds which were both backward-curved centrifugal fans located in the product and working air outlet ducts. The product and exhaust air flow volumes were calculated by measuring the static pressure drop across converging-diverging nozzles. The air flow volumes were then calculated as:

$$Q = k \cdot \sqrt{\rho_s/\rho \cdot \Delta P} \tag{1}$$

where Q is the volumetric air flow rate in m^3/h, k is the nozzle calibration factor which is relevant to the inlet nozzles, ΔP is the static pressure drop across the nozzle in Pa, ρ_s is the standard air density of 1.2 kg/m^3, and ρ is the actual air density in kg/m^3.

The pressure drops were measured using micro manometers (measurement range: 0–2000 Pa, accuracy: 10 Pa). The exhaust air was discharged to the outdoor through a duct, which gave an additional flow resistance. Thus, a variable-speed supplement fan was installed at the duct outlet to maintain the static pressure at room pressure at the dew-point evaporative cooler outlet. The temperature and humidity of the incoming air, product air and exhaust air were all measured using temperature and humidity sensors (HC2A-S, accuracy: ±0.1 °C, ±0.8% RH). The water temperature was measured using an RTD (accuracy: ±0.2 °C). The volumetric water flow was measured by a water flow meter (measurement range: 12.5–600 L/h, accuracy ±5%). The power consumption of the fans and water pump were measured by power meters (accuracy: ±0.5%).

2.3. Performance parameters

The cooling of a dew-point evaporative cooler is usually evaluated by the cooling efficiency and the coefficient of performance. The cooling efficiency can be denoted by the wet-bulb efficiency, ε_{wb}, and dew-point efficiency, ε_{dp}, with the energy efficiency usually given by the coefficient of performance (COP).

$$\varepsilon_{wb} = \frac{t_{db,in} - t_{db,out}}{t_{db,in} - t_{wb,in}} \tag{2}$$

$$\varepsilon_{dp} = \frac{t_{db,in} - t_{db,out}}{t_{db,in} - t_{dp,in}} \tag{3}$$

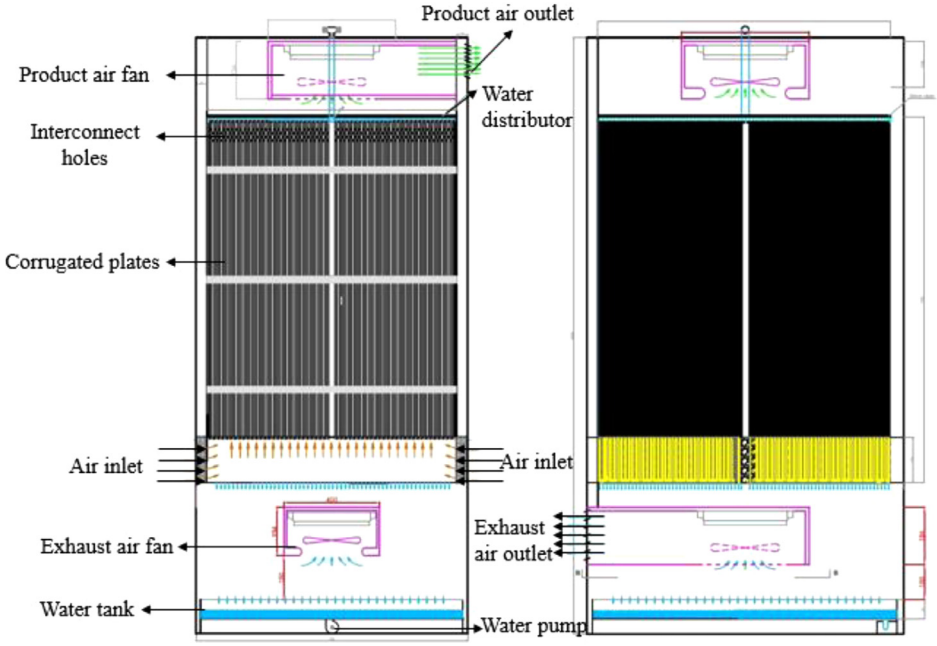

Fig. 2. Dew-point evaporative cooler system design.

$$COP = \frac{Q_{cooling}}{\mathrm{Pw}} \tag{4}$$

$$Q_{cooling} = m_{a,in} \cdot c_{p,a}(1-r) \cdot \left(t_{db,in} - t_{db,out}\right) \tag{5}$$

2.4. Uncertainty of the experimental results

The relative uncertainties of the volumetric air flow rate, cooling capacity, cooling efficiency and COP were calculated from the measured temperatures and humidities as:

$$\frac{\Delta y}{y} = \sqrt{\sum_i \left(\frac{\partial y}{\partial x_i} \cdot \frac{\Delta x_i}{y}\right)^2} \tag{6}$$

where y is one of the calculated parameters and x represents the directly measured values.

The calculation results showed that the highest relative uncertainty of the product air temperature was ±0.6%, highest relative uncertainty of the air flow volume was ±6.3%, the highest relative uncertainty of the cooling capacity was ±6.4%, the relative uncertainty of the COP was ±6.42%, the relative uncertainty of the cooling efficiency was ±1.7%.

3. Numerical model

3.1. Mathematical modeling

The physical model was based on half of the dry channel and half of the wet channel in the x-y plane as shown in Fig. 5. The heat transfer in the dry channel and the heat and mass transfer in the wet channel are related through the energy, momentum and diffusion equations for the primary air, water and working air. The model was based on the following assumptions:

(a) The heat and mass transfer are at steady state.
(b) There is no heat transfer to the surroundings from the exchanger.
(c) The wet channel wall is completely wetted by water.
(d) The air flow in the wet channel is uniform [36].
(e) The gravitational terms are negligible in the air momentum equations.

For primary air in the dry channel:
Mass equation:

$$\rho_d \nabla \cdot \left(\vec{u}_d\right) = 0 \tag{7}$$

Momentum equation:

$$\rho_d\left(\vec{u}_d \cdot \nabla\right)\vec{u}_d = \nabla \cdot \left[-p_d\vec{I} + \mu_d\left(\nabla\vec{u}_d + \left(\nabla\vec{u}_d\right)^T\right)\right] \tag{8}$$

Energy equation:

$$\rho_d c_{p,d}\vec{u}_d \cdot \nabla t_d = \nabla \cdot (k_d \nabla t_d) + \phi_d \tag{9}$$

where,

$$\phi_d = 2\frac{h_t(t_f - t_d)}{l_d} \tag{10}$$

h_t is calculated as:

$$h_t = \frac{1}{\frac{1}{h_d} + \frac{\delta_{pl}}{k_{pl}} + \frac{1}{h_f}} \tag{11}$$

For water, the momentum and heat transfer equations lead to [37]:

$$\delta_f = \left(\frac{3\nu_f \Gamma}{\rho_f g}\right)^{1/3} \tag{12}$$

Where,

$$\Gamma = \frac{m_f}{(n+1)W} \tag{13}$$

The heat transfer coefficient for the falling water film is given by [37]:

$$Nu_f = \frac{h_f \delta_f}{k_f} = 1.88 \tag{14}$$

The energy equation for the water film is:

$$\rho_f c_{p.f}\vec{u}_f \cdot \nabla t_f = \nabla \cdot (k_f \nabla t_f) + \phi_f \tag{15}$$

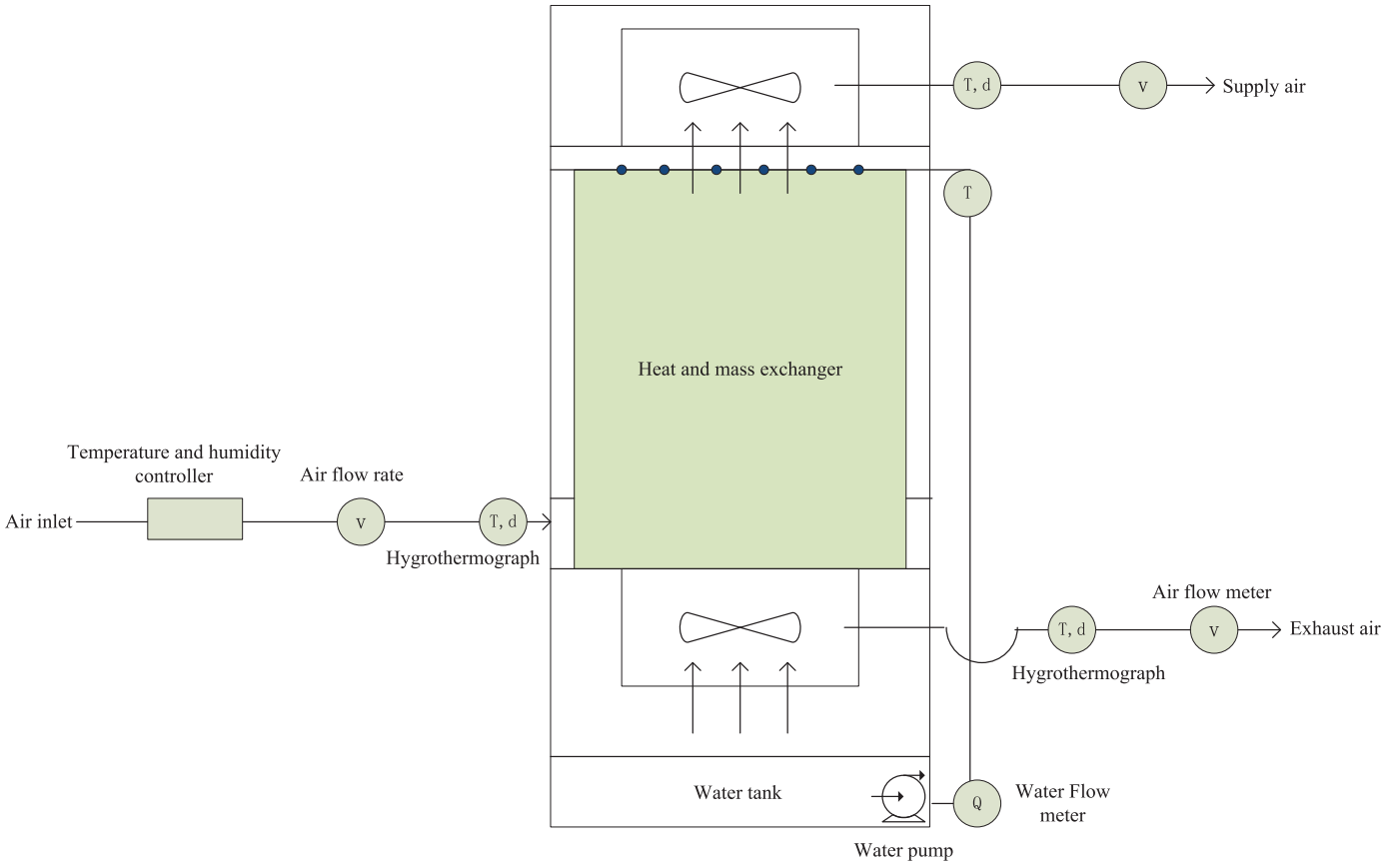

Fig. 3. Test system schematic.

where,

$$\phi_f = \frac{h_t(t_d - t_f)}{\delta_f} + \frac{h_w(t_w - t_f)}{\delta_f} - \frac{h_m(d_s - d_w)\rho_{a,w}}{\delta_f} h_{la} \tag{16}$$

where d_s(kg/kg) is the humidity of the wet air at the water film surface where the partial pressure of the water vapour is equal to the saturation pressure at the water film temperature and can be calculated as:

$$d_s = 0.622 \frac{p_s}{p_t - p_s} \tag{17}$$

where P_t is the total pressure of air and P_s is the saturation pressure of the water vapour which can be calculated using the correlation proposed by Goff-Gratch [38],

$$\log(p_s) = c1(T^* - 1) + c2\log(T^*) + c3\left(10^{c4\left(1-\frac{1}{T^*}\right)} - 1\right) + c5\left(10^{c6(T^*-1)} - 1\right) + c7 \tag{18}$$

where

$$T* = \frac{373.16}{T_f} \tag{19}$$

c1 = −7.90298, c2 = 5.02808, c3 = -1.3816×10^{-7}, c4=11.344, c5 = 8.1328×10^{-3}, c6 = −3.49149, and c7 = log (1013.246)

For the working air in the wet channel:

Energy equation:

$$\rho_w c_{p,w} \vec{v}_w \cdot \nabla t_w = \nabla \cdot (k_w \nabla t_w) + \phi_w \tag{20}$$

where,

$$\phi_w = 2\frac{h_w \cdot (t_f - t_w)}{l_w} - h_v(t_w) \cdot \vec{v}_w \frac{\partial d_w}{\partial y} \cdot \rho_{a,w} + 2\frac{h_m(d_s - d_w) \cdot \rho_{a,w}}{l_w} \cdot h_v(t_f) \tag{21}$$

The moisture transport in the air equation is:

$$\vec{v}_w \cdot \nabla d_w = \nabla \cdot (D_{ab} \nabla d_w) + \phi_m \tag{22}$$

where,

$$\phi_m = 2\frac{h_m \cdot (d_s - d_w)}{l_w} \tag{23}$$

The heat transfer coefficient of the air in the wet channel is calculated using the equation proposed by Dowdy et al. [39] which was obtained from the experiment results of evaporative cooling with the surface covered by a rigid cellulose media saturated with water:

$$Nu = 0.1\left(\frac{l_e}{\delta_{po}}\right)^{0.12} \mathrm{Re}^{0.8} \mathrm{Pr}^{1/3} \tag{24}$$

$$l_e = \frac{V}{A} \tag{25}$$

The mass transfer coefficient is then calculated using the Lewis correlation as

$$\frac{h_w}{h_m} = c_{p,w} Le^{2/3} \tag{26}$$

The convective heat transfer coefficient of the primary air in the dry channel is calculated using the correlation proposed by Awad [40] which applies to high width-to-height square channels which is widely used in heat and mass exchangers for dew-point evaporative coolers.

$$Nu = \left[\left(1.490 \cdot y^{*-1/3}\right)^{4.5} + 8.235^{4.5}\right]^{(1/4.5)} \tag{27}$$

Fig. 4. Dew-point evaporative cooler test system.

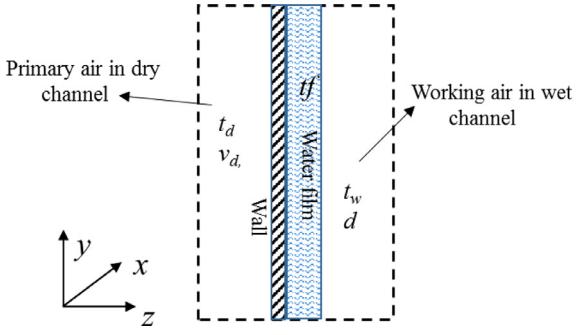

Fig. 5. Physical model of the dew-point evaporative cooler.

where y^* is the dimensionless length.

$$y^* = y/(\mathrm{DeRePr}) \tag{28}$$

3.2. Boundary conditions

Boundary conditions for the primary air in the dry channel:
Inlet:

$$t_d = t_{d,in}, u_d = u_{in}, v_d = 0 \tag{29}$$

Outlet:

$$P = 0, \frac{\partial t_d}{\partial y} = 0 \tag{30}$$

The wall is assumed to be adiabatic:

$$u = v = 0, \frac{\partial t_d}{\partial x} = 0 \tag{31}$$

Boundary conditions for the working air in the wet channel:

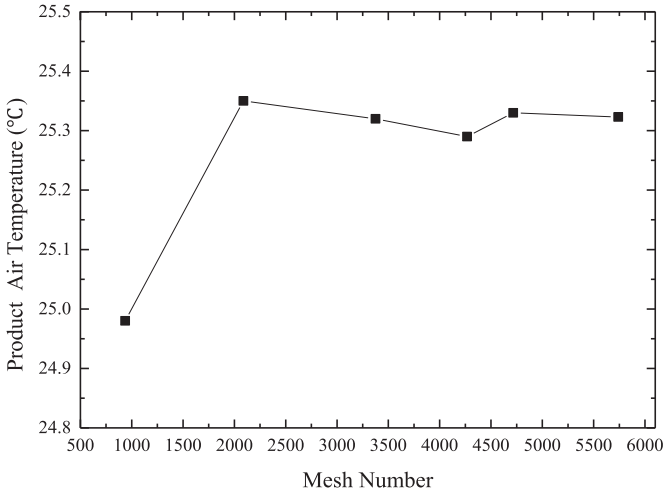

Fig. 6. Grid independent check.

Inlet:

$$t_{w,in} = t_{d,out}, d_{w,in} = d_{d,in} \tag{32}$$

Outlet:

$$\frac{\partial t_w}{\partial y} = 0, \frac{\partial d_w}{\partial y} = 0 \tag{33}$$

The working air flow in the wet channel is assumed to be uniform.

$$u_w = 0, |v_w| = \left|\vec{u}_d\right| \cdot r \tag{34}$$

Boundary conditions for the water flow in the wet channel:
Inlet:

$$t_f = t_{f,in} \tag{35}$$

Outlet:

$$\frac{\partial t_f}{\partial y} = 0 \tag{36}$$

3.3. Simulation method

The governing equations for the primary air, working air and water film are coupled, so all the equations were solved simultaneously. The primary air flow in the dry channel was assumed to be laminar flow because of the low Reynolds number. The governing equations were discretized using the finite element method and solved using COMSOL. The mesh was generated in COMSOL and the grid independent was checked for each case. One of the grid independent checks is shown in Fig. 6.

4. Experimental results and model validation

4.1. Model validation

The experiments were run for the various operating conditions listed in Table 2, where the highest relative uncertainty of the product air temperature was ±0.6%. All the experimental results in Table 2 are compared with the numerical results in Fig. 7 which shows that the numerical results agreed well with the experimental results for the dew-point evaporative cooler. The numerical model was further validated for various dew-point evaporative cooler designs against the experimental results of Riangvilaikul and Kumar [10] and Duan et al. [41] shown in Figs. 8 and 9. The relative error between the numerical and experimental results were all within 3%.

Table 2
Experimental data.

Test No	Incoming air temperature/relative humidity °C/%	Water temperature °C	Water volumetric flow rate L/h	Primary air volumetric flow rate m^3/h	Working air volumetric flow rate m^3/h	Working-to-primary air flow ratio	Product air temperature °C	Wet-bulb efficiency	Dew-point efficiency	Cooling capacity W	COP
1	38.3/25.4%	26	960	3153	1272	0.403	23.4	95.5%	64.8%	9534	27.2
2	38.1/25%	26	960	2928	1279	0.437	23	96.2%	65.1%	8470	27.6
3	38.1/25%	26	360	2928	1279	0.437	22.5	96.9%	64.7%	8751	30.3
4	38.1/23.7%	26	384	2972	1323	0.445	22.1	99.4%	66.4%	8975	31
5	38.4/21.4%	25.2	864	2839	1314	0.463	22.3	95.5%	62.6%	8353	31.4
6	38.4/20.5%	25.2	768	2788	1263	0.453	21.7	97.7%	63.5%	8664	33.1
7	38.8/17.7%	24.4	768	2797	1272	0.455	20.7	99.6%	63.3%	9391	35.6
8	38.6/17%	24	768	2719	1188	0.437	20.4	96.3%	59.3%	9267	36.6
9	37.6/15.9%	24.5	768	3236	1232	0.381	21.3	89.2%	54.4%	11,108	30.7
10	37.8/15.9%	23.9	960	2434	1304	0.536	20.2	95.9%	58.7%	8074	31.4
11	25.4/29%	20	960	2112	974	0.461	17.2	74.9%	42.9%	3173	20
12	38.4/29.4%	25	960	3182	1150	0.361	24.4	96.6%	71.4%	9676	23.8
13	38.6/24.6%	25	960	2732	1261	0.462	22.5	100.6%	68.2%	8054	30.5
14	37.3/34.6%	25	960	2621	1173	0.447	24	103.9%	73.9%	6551	24.8
15	38.3/33.8%	25	960	2914	1150	0.395	24	107.5%	77.3%	8582	30.1
16	38.7/33.8%	27	960	3195	1284	0.402	25.4	99.3%	71.5%	8647	24.6
17	37.6/32.9%	27	960	3285	1286	0.391	25.1	99.3%	71.1%	9181	22.6

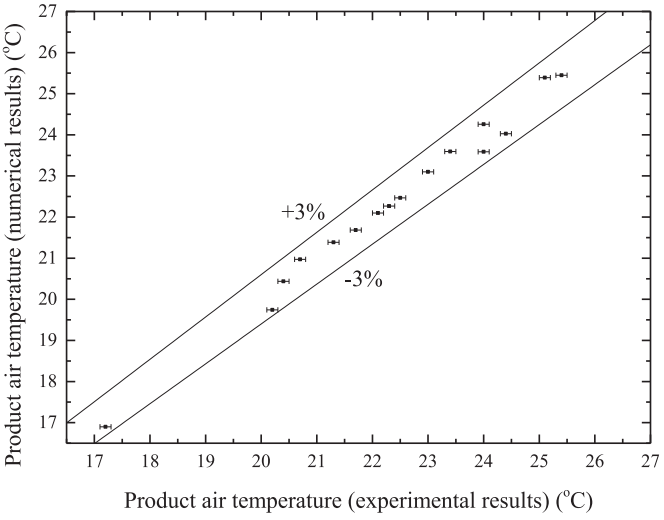

Fig. 7. Comparison of the numerical results with the current experimental data.

4.2. Experimental results discussion

Comparisons of the experimental results of tests 1 and 2, 3 and 4, and 12 and 13 show that the product air temperature decreases with increasing working-to-primary air ratio. The reason is that the heat and mass transfer coefficients of the working air increase with increasing working air flow rate as which can deduced from Eq. (24). However, the cooling capacity did not always increase because reducing the product air flow rate and reducing the product air temperature cause the cooling capacity to change in opposite directions.

Comparisons of the experimental results of tests 2 and 3 and 5 and 6 show that the product air temperature decreases with decreasing water volumetric flow rate for a given inlet water temperature. Comparison of the experimental results of tests 6, 7 and 8 shows that the product air temperature decreases with decreasing water temperature for a given volumetric water flow rate. These influences of the water on the cooling of dew-point evaporative coolers agree with the effects seen in the numerical study by Liu et al. [36].

The highest wet-bulb efficiency among the listed tests was 107.5% while the highest dew-point efficiency was 77.3%. The experimental results show that the cooling efficiency can be improved by decreasing the volumetric water flow rate and the inlet water temperature and increasing the working-to-primary air ratio.

During the tests, an interesting phenomenon was found after the water pump was turned off that the product air temperature decreased to a minimum and then increased again. Two sets of temperature data for the product air, incoming air and water after the water pump was turned off are shown in Figs. 10 and 11 In test 4 with a product air temperature of 22.1°C and a volumetric water flow rate of 384 L/h, after the water pump was turned off at time of 09:31, the product air temperature first decreased to 20.9°C and then increased again as the wet surface slowly dried. After the water pump was turned on again, the product air temperature again remained constant at 22.3°C (Test 5). The product air temperatures again decreased after the water pump was turned off after test 5 and test 8. The lowest product air temperature is 17.8°C as shown in Fig. 11, where the cooling capacity is 10,829 W, the wet-bulb efficiency is 114%, the dew-point efficiency is 68% and the COP is 42.8 for the conditions of test 8 which is the design operating conditions. Also, the wet-bulb efficiency can be higher than 138% when the working-to-primary air ratio is 0.7, but the cooling capacity and COP are both relatively low.

The product temperature initially decreases after the water pump is turned off because there is still the water in the porous layer of the wet channel surface, and the water film thickness is decreasing with time because of the flow and evaporation, which will reduce the thermal resistance of the water film. When there is not enough water to wet the surface, the heat and mass transfer will decrease and the product air temperature will rise. So, there must be a best water flow volume for a given water temperature as discussed in [36].

4.3. Comparison between the existed commercial dew-point evaporative cooler and the present one

The cooling performance of the Coolerado M30 which is arranged as cross flow for air and water was studied in the lab. The comparison between the M30 and the present prototype is shown in Table 3. It is seen that under the similar conditions, the wet-bulb efficiency and COP are both improved obviously with

Table 3
Comparison of the present prototype with the M30.

Cooler	Primary air flow rate (m^3/h)	Working air flow rate (m^3/h)	Ratio	Inlet air dry-bulb temperature (°C)	Inlet air wet-bulb temperature (°C)	Product air temperature (°C)	Cooling capacity (kW)	Wet-bulb efficiency	COP
M30	4522	2363	0.523	37.78	21.11	22	11.77	94.5%	28.9
	3349	1615	0.482	37.78	18.33	20.94	10.08	88.2%	31.8
Prototype	2719	1188	0.437	38.6	20.28	17.8	10.83	114%	42.8
	2972	1323	0.445	38.1	22.03	20.9	9.65	107%	33.3

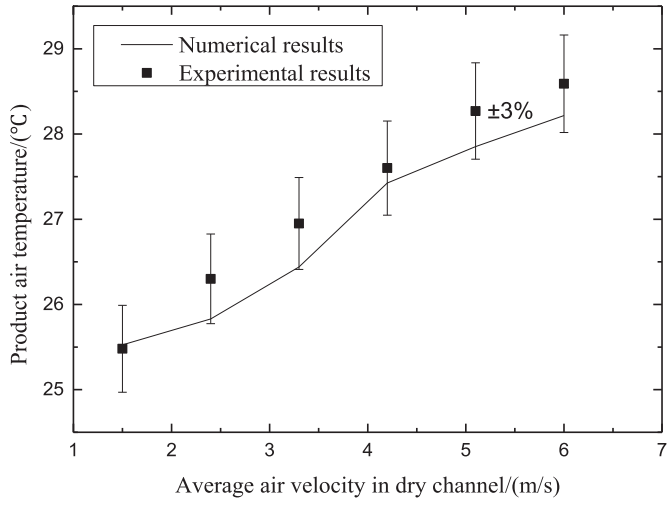

(a) Incoming air conditions: 34°C and 19 g/kg

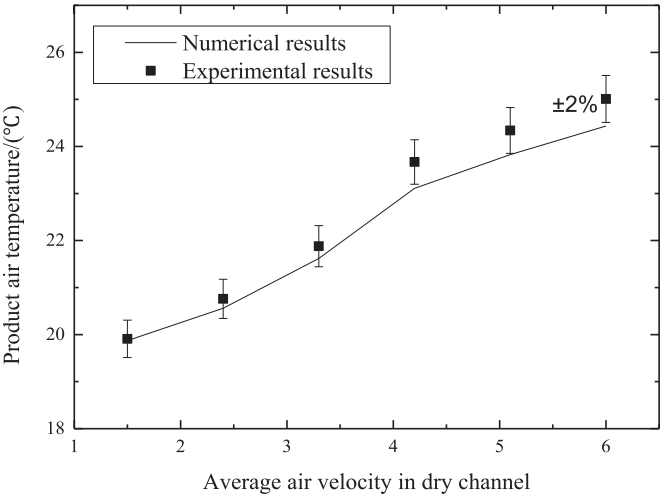

(b) Incoming air conditions: 34°C and 11.2 g/kg

Fig. 8. Model validation against experimental results from Riangvilaikul and Kumar [10].

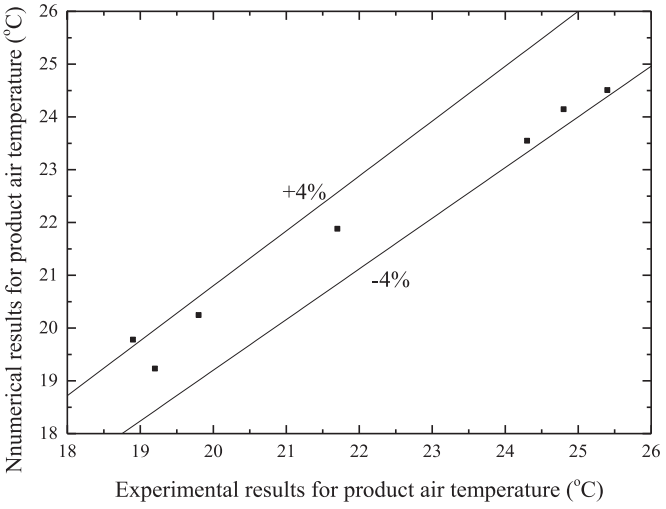

Fig. 9. Model validation against experimental results from Duan et al. [41].

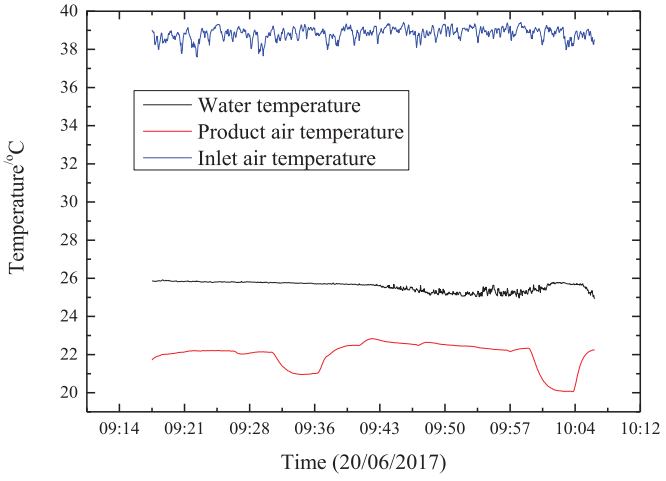

Fig. 10. Temperature variations with time after the water pump was turned off after test 4.

similar cooling capacity for the present prototype compared to the M30 though the primary air flow rate and working air flow rate of the present prototype are both smaller than of the M30. For the M30 with cooling capacity 10.08 kW and the present prototype with cooling capacity 10.83 kW, the cooling efficiency of the present prototype is improved by 29.3% (from 88.2% to 114%) and the COP of the present prototype is improved by 34.6% (from 31.8 to 42.8) with smaller air flow rate of the present prototype for the similar inlet air parameters.

5. Numerical results and discussion

The numerical model was verified against the experimental results from this and other studies. The influence of the structure on the dew-point evaporative cooler is difficult to study experimentally, but can be easily studied numerically. Therefore, the dew-point evaporative cooler design was improved to increase the cooling by using the numerical model to study the influences of various design parameters on the dew-point evaporative cooler cooling capability.

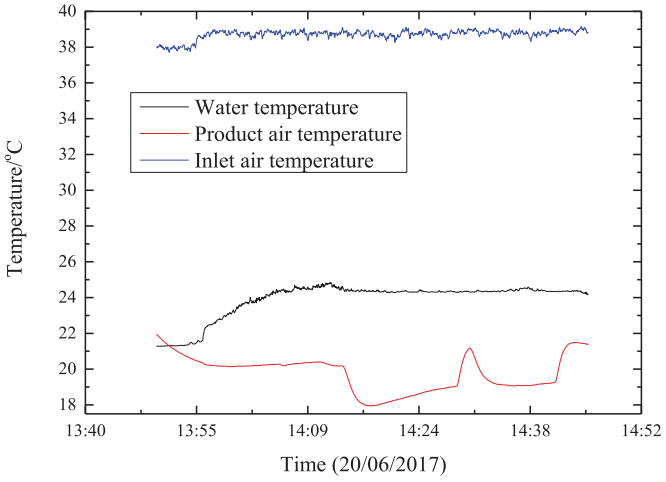

Fig. 11. Temperature variations with time after the water pump was turned off after test 8.

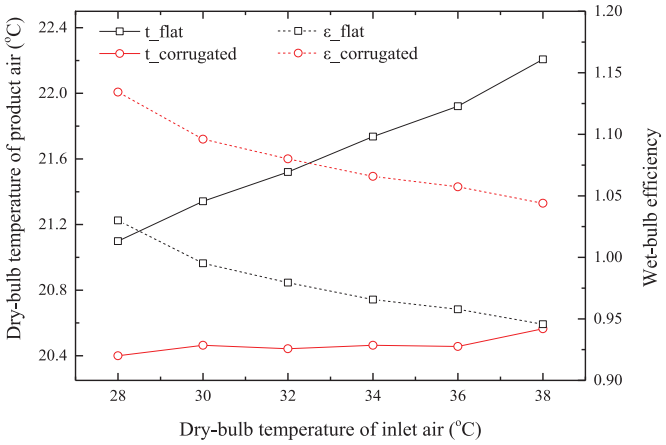

Fig. 12. Dew-point evaporative coolers with corrugated and flat plates.

5.1. Comparison between dew-point evaporative coolers with flat plates and corrugated plates

Fig. 12 compares the product air temperatures and wet-bulb efficiencies of dew-point evaporative coolers with corrugated plates and with flat plates for various inlet air conditions for an average primary air velocity of 2 m/s, working-to-primary air ratio of 0.44, water flow rate of 0.48 L/h per cooling unit and water inlet temperature of 20°C. The wet-bulb efficiency of the cooler with the corrugated plates is over 10% higher than that with the flat plates.

The corrugated plates improve the cooling efficiency by increasing the cooler surface area and by increasing the heat and mass transfer coefficients. Thus, the corrugated plates are a simple and efficient way to improve the cooling capability of the dew-point evaporative cooler instead of flat plates.

5.2. Influence of channel length

The influence of the channel length on the cooling efficiency of the dew-point evaporative cooler is shown in Fig. 13 for the same operating conditions as in Section 5.1. The phenomenon that the cooling efficiency is improved by increasing the channel length is easy to understand. A longer channel give more time for heat and mass transfer in the dew-point evaporative cooler. However, a longer channel also gives a larger air flow resistance (which leads to a higher fan power), higher material costs and a larger volume.

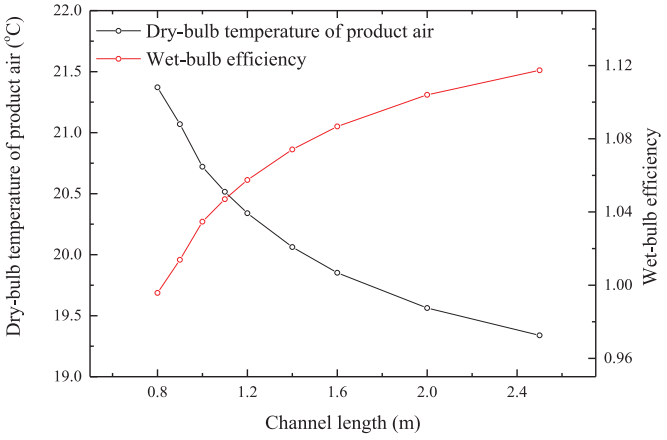

Fig. 13. Influence of channel length on the cooling efficiency.

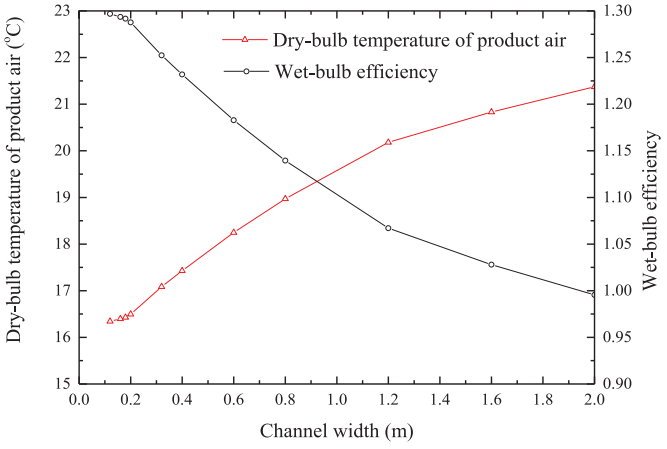

Fig. 14. Influence of channel width on the cooling efficiency.

In addition, the cooling efficiency improvements brought by the increasing channel length become smaller with increasing channel length as shown in Fig. 13. Thus, the optimal channel length should be chosen based on the specific requirements of the conditioned space.

5.3. Influence of channel width

The influence of channel width on the cooling efficiency of the dew-point evaporative cooler is shown in Fig. 14 for the same operating conditions as in Section 5.1. The channel width influences the air flow in the dry channel, because the incoming air enters into the dew-point evaporative cooler from below the plate and flows out of the cooler from the top as shown in Fig. 2. The cooling efficiency increases with decreasing channel width because the air flow is more uniform in a dry channel with a smaller channel width. However, a smaller channel width means a smaller volumetric air flow rate which will leads to a smaller cooling capacity. Also, the results in Fig. 15 then show that the best working-to-primary air ratio that gives the highest cooling capacity varies with the channel width.

5.4. Influence of channel gap width

The influence of the channel gap on the cooling efficiency of the dew-point evaporative cooler shown in Fig. 16 shows that the cooling efficiency increases with decreasing channel gap. As the channel gap width decreases, the volumetric air flow in each cooling unit decreases, so the air temperature decreases when the

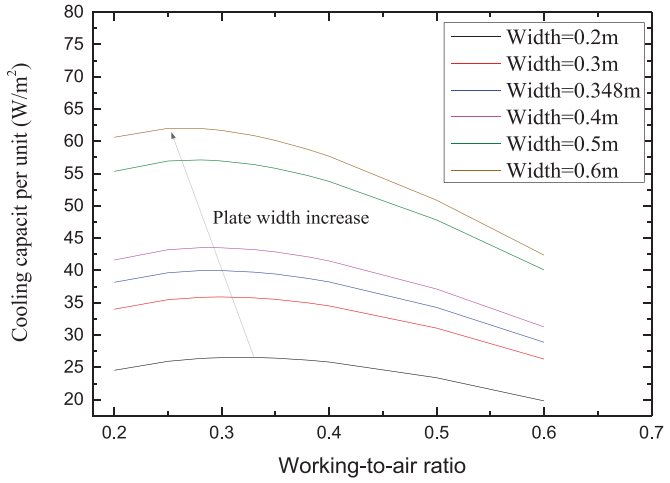

Fig. 15. Influence of working-to-primary air ratio for various channel widths.

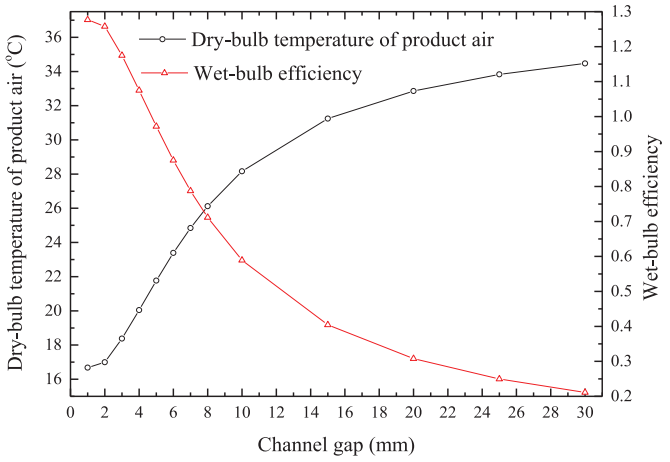

Fig. 16. Influence of channel gap on the cooling efficiency.

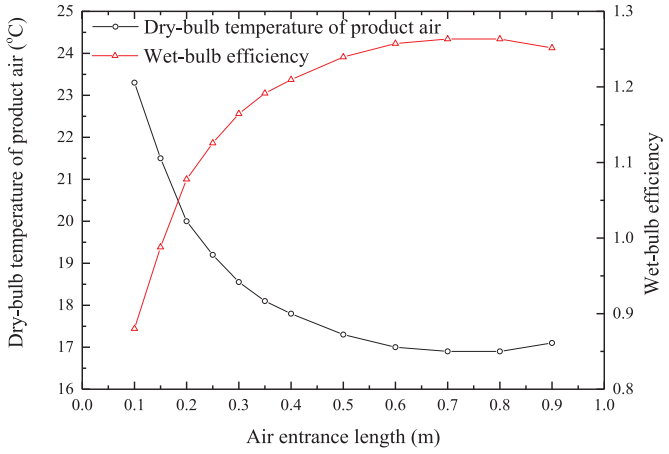

Fig. 17. Influence of air inlet length on the cooling efficiency.

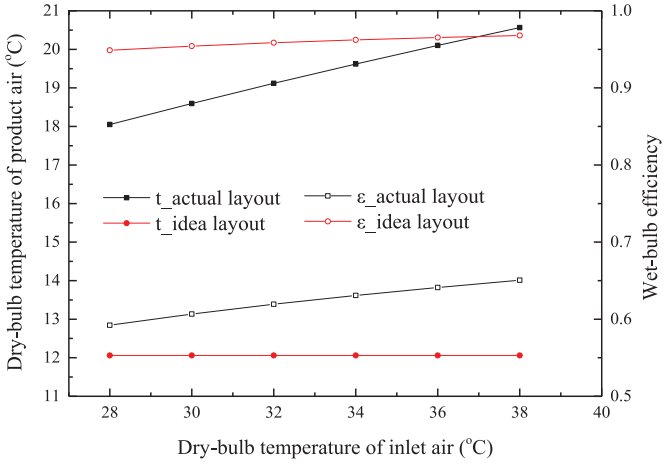

Fig. 18. Comparison of various air flow arrangements.

total heat transfer for each cooling unit does not change a lot. But when the channel gap width decreases, the same total volumetric air flow of the cooler would then require more plates and the resulting dew-point evaporative cooler would be heavier. Also, for channel gaps smaller than 4 mm, the cooling efficiency increases become quite small as the channel gap further decreases.

5.5. Influence of air inlet arrangement

For the dew-point evaporative cooler analyzed in this study, the incoming air enters the dry channel from the bottom along a flat plate and flows along the dry channels in the corrugated plate, so the air inlet design strongly influences the air distribution. When the inlet length is less than 0.6 m, the cooling efficiency increases as the air inlet length increases as shown in Fig. 17. Since the air inlet cannot be arranged exactly at the bottom of the cooler due to the air and water separation method as shown in Fig. 2, the air flow in the dew-point evaporative cooler is not exactly counter flow. The cooling efficiency difference between the actual flow and an ideal counter flow pattern is shown in Fig. 18 which shows that the cooling efficiency of the dew-point evaporative cooler with the actual flow arrangement is only 62%–67% of that with the ideal counter-flow arrangement. Thus, the cooling efficiency can be significantly improved by optimizing the dew-point evaporative cooler design.

6. Conclusions

This paper investigated the cooling performance of a high-efficiency dew-point evaporative cooler using the combined experimental and numerical simulation method. This cooler, characterized by the enhanced cooling effectiveness and significantly improved energy efficiency, can achieve 34.6% higher COP and 29.3% higher wet-bulb efficiency compared to the existing commercial dew-point evaporative cooler of the same capacity. An improved two-dimensional, multi-factor engaged numerical model where the air momentum equation and water flow equation are included and solved simultaneously with the air energy and mass transfer equations, and specific heat and mass transfer correlations for wet air is adopted in the energy and mass transfer equations, featured with advantages of improved accuracy and extended applicability, was developed and verified with experimental results and was used to optimize the dew-point evaporative cooler structure.

The testing results showed that the selected experimental dew point air cooler can achieve the wet-bulb efficiency of 114% and dew-point efficiency of 68.4%, cooling capacity of 10,829 W and maximum COP of 42.8 under the standard operational condition. The volumetric water flow rate and the inlet water temperature can be appropriately adjusted to give the best cooling output.

The numerical results showed that the cooling efficiency of the dew-point evaporative cooler with corrugated plates is more than 10% higher than with flat plates. The cooling efficiency of the dew-point evaporative cooler with the actual flow arrangement is

only 62%–67% of the dew-point evaporative cooler with an ideal counter-flow arrangement. The cooling efficiency can be improved by increasing the channel length and the air inlet length and reducing the channel width and the channel gap within a reasonable range. The optimal parameters should be chosen based on the specific requirements of the conditioned space.

Conflict of interest statement

We declare that we have no financial and personal relationships with other people or organizations that can inappropriately influence our work, there is no professional or other personal interest of any nature or kind in any product, service and/or company that could be construed as influencing the position presented in, or the review of, the manuscript entitled, “Experimental and Numerical Investigation of a High-efficiency Dew-point Evaporative Cooler”.

Acknowledgements

This work was supported by the National Key R&D Program of China (Grant No. 2016YFE0133300), European Commission H2020 MSCA Programme (for the EU H2020—MSCA-RISE-2016-734340–DEW-COOL-4-CDC project), the Royal Academy of Engineering (for the UK-CIAPP\415 project).

References

[1] G.P. Maheshwari, F. Al-Ragom, R.K. Suri, Energy-saving potential of an indirect evaporative cooler, Appl. Energy 69 (1) (2001) 69–76.
[2] Z. Duan, C. Zhan, X. Zhang, M. Mustafa, X. Zhao, B. Alimohammadi Sagvand, A. Hasan, Indirect evaporative cooling: past, present and future potentials, Renew. Sustain. Energy Rev. 16 (9) (2012) 6823–6850.
[3] V. Maisotsenko, L.E. Gillan, T.L. Heaton, A.D. Gillan, Method and Plate Apparatus for DewPoint Evaporative Cooler, 2003 F25D17/06;F28C1/00; F28D5/00ed. United States.
[4] L. Elberling, Laboratory Evaluation of the Coolerado Cooler-Indirect Evaporative Cooling Unit, Pacific Gas and Electric Company, 2006.
[5] Idalex, The Maisotsenko Cycle—Conceptual. A Technical Concept View of the Maisotsenko Cycle, 2003.
[6] S.T. Hsu, Z. Lavan, W.M. Worek, Optimization of wet-surface heat exchangers, Energy 14 (11) (1989) 757–770.
[7] J. Lee, B.S. Choi, D.Y. Lee, Comparison of configurations for a compact regenerative evaporative cooler, Int. J. Heat Mass Transfer 65 (5) (2013) 192–198.
[8] C. Zhan, Z. Duan, X. Zhao, S. Smith, H. Jin, S. Riffat, Comparative study of the performance of the M-cycle counter-flow and cross-flow heat exchangers for indirect evaporative cooling–paving the path toward sustainable cooling of buildings, Energy 36 (12) (2011) 6790–6805.
[9] B. Riangvilaikul, S. Kumar, Numerical study of a novel dew point evaporative cooling system, Energy Build. 42 (11) (2010) 2241–2250.
[10] B. Riangvilaikul, S. Kumar, An experimental study of a novel dew point evaporative cooling system, Energy Build. 42 (5) (2010) 637–644.
[11] A.E. Kabeel, M. Abdelgaied, Numerical and experimental investigation of a novel configuration of indirect evaporative cooler with internal baffles, Energy Convers. Manag. 126 (2016) 526–536.
[12] J. Lee, D.Y. Lee, Experimental study of a counter flow regenerative evaporative cooler with finned channels, Int. J. Heat Mass Transfer 65 (5) (2013) 173–179.
[13] P. Xu, X. Ma, X. Zhao, K. Fancey, Experimental investigation of a super performance dew point air cooler, Appl. Energy 203 (2017) 761–777.
[14] S. Anisimov, D. Pandelidis, Numerical study of the Maisotsenko cycle heat and mass exchanger, Int. J. Heat Mass Transfer 75 (4) (2014) 75–96.
[15] S. Anisimov, D. Pandelidis, J. Danielewicz, Numerical analysis of selected evaporative exchangers with the Maisotsenko cycle, Energy Convers. Manag. 88 (2014) 426–441.
[16] S. Anisimov, D. Pandelidis, A. Jedlikowski, V. Polushkin, Performance investigation of a M (Maisotsenko)-cycle cross-flow heat exchanger used for indirect evaporative cooling, Energy 76 (2014) 593–606.
[17] Pandelidis, S. Anisimov, Numerical analysis of the heat and mass transfer processes in selected M-Cycle heat exchangers for the dew point evaporative cooling, Energy Convers. Manag. 90 (2015) 62–83.
[18] D. Pandelidis, S. Anisimov, W.M. Worek, Comparison study of the counter-flow regenerative evaporative heat exchangers with numerical methods, Appl. Therm. Eng. 84 (2015) 211–224.
[19] D. Pandelidis, S. Anisimov, Numerical analysis of the selected operational and geometrical aspects of the M-cycle heat and mass exchanger, Energy Build. 87 (3) (2015) 413–424.
[20] S. Anisimov, D. Pandelidis, J. Danielewicz, Numerical study and optimization of the combined indirect evaporative air cooler for air-conditioning systems, Energy 80 (2) (2015) 452–464.
[21] D. Pandelidis, S. Anisimov, Numerical study and optimization of the cross-flow Maisotsenko cycle indirect evaporative air cooler, Int. J. Heat Mass Transfer 103 (2016) 1029–1041.
[22] Robichaud, R. Coolerado Cooler Helps to Save Cooling Energy and Dollars: New Cooling Technology Targets Peak Load Reduction. United States. doi:10.2172/908968.
[23] L. Elberling, Laboratory evaluation of the Coolerado Cooler-indirect evaporative cooling unit, Pac. Gas Electric Comp. (2006).
[24] X. Zhao, J.M. Li, S.B. Riffat, Numerical study of a novel counter-flow heat and mass exchanger for dew point evaporative cooling, Appl. Therm. Eng. 28 (14–15) (2008) 1942–1951.
[25] X. Cui, K.J. Chua, W.M. Yang, Numerical simulation of a novel energy efficient dew point evaporative air cooler, Appl. Energy 136 (2014) 979–988.
[26] X. Cui, K.J. Chua, W.M. Yang, K.C. Ng, K. Thu, V.T. Nguyen, Studying the performance of an improved dew-point evaporative design for cooling application, Appl. Therm. Eng. 63 (2) (2014) 624–633.
[27] J. Lin, K. Thu, T.D. Bui, R.Z. Wang, K.C. Ng, K.J. Chua, Study on dew point evaporative cooling system with counter-flow configuration, Energy Convers. Manag. 109 (2016) 153–165.
[28] J. Lin, K. Thu, T.D. Bui, R.Z. Wang, K.C. Ng, M. Kumja, K.J. Chua, Unsteady-state analysis of a counter-flow dew point evaporative cooling system, Energy 113 (2016) 172–185.
[29] A. Hasan, Indirect evaporative cooling of air to a sub-wet bulb temperature, Appl. Therm. Eng. 30 (16) (2010) 2460–2468.
[30] A. Hasan, Going below the wet-bulb temperature by indirect evaporative cooling: analysis using a modified ε-NTU method, Appl. Energy 89 (1) (2012) 237–245.
[31] F. Bruno, On-site experimental testing of a novel dew point evaporative cooler, Energy Build. 43 (12) (2011) 3475–3483.
[32] L. Bellemo, B. Elmegaard, L.O. Reinholdt, M.R. Kærn, Modeling of a regenerative indirect evaporative cooler for a desiccant cooling system, 4th IIR Conference on Thermophysical Properties and Transfer Processes of Refrigerants, 2013.
[33] E. Rogdakis, I. Koronaki, D.N. Tertipis, A. Mustafa, An energy evaluation of a maisotsenko evaporative cooler based on cylinder geometry, World Acad. Sci. Eng. Technol. 82 (2013) 347–356.
[34] E.D. Rogdakis, I.P. Koronaki, D.N. Tertipis, Experimental and computational evaluation of a Maisotsenko evaporative cooler at Greek climate, Energy Build. 70 (2014) 497–506.
[35] M. Jradi, S. Riffat, Experimental and numerical investigation of a dew-point cooling system for thermal comfort in buildings, Appl. Energy 132 (2014) 524–535.
[36] Y. Liu, J.M. Li, X. Yang, X. Zhao, Two-dimensional numerical study of a heat and mass exchanger for a dew-point evaporative cooler, Energy 168 (2019) 975–988.
[37] N.J. Stoitchkov, G.I. Dimitrov, Effectiveness of crossflow plate heat exchanger for indirect evaporative cooling: efficacité des échangeurs thermiques à plaques, à courants croises pour refroidissement indirect évaporatif, Int. J. Refrig. 21 (6) (1998) 463–471.
[38] X.U. Junzeng, Q. Wei, S. Peng, Y.U. Yanmei, Error of saturation vapor pressure calculated by different formulas and its effect on calculation of reference evapotranspiration in high latitude cold region, Procedia Eng. 28 (2012) 43–48.
[39] J.A. Dowdy, R.L. Reid, E.T. Handy, Experimental determination of heat- and mass-transfer coefficients in aspen pads, ASHRAE Trans. 92 (1986).
[40] M.M. Awad, Heat transfer for laminar thermally developing flow in parallel–plates using the asymptotic method, in: Thermal Issues in Emerging Technologies Theory and Applications (ThETA), 2010 3rd International Conference, IEEE, 2010, pp. 371–387.
[41] Z. Duan, C. Zhan, X. Zhao, X. Dong, Experimental study of a counter-flow regenerative evaporative cooler, Build. Environ. 104 (2016) 47–58.